

Stress testing Λ CDM with high-redshift galaxy candidates

Michael Boylan-Kolchin^{*}

Department of Astronomy, The University of Texas at Austin, 2515 Speedway, Stop C1400, Austin, TX 78712-1205, USA

Draft version, 2 August 2022

ABSTRACT

Early data from *JWST* have revealed a bevy of high-redshift galaxy candidates with unexpectedly high stellar masses. I examine these candidates in the context of the most massive galaxies expected in Λ CDM-like models, wherein the stellar mass of a galaxy is limited by the available baryonic reservoir of its host dark matter halo. For a given cosmology, the abundance of dark matter halos as function of mass and redshift sets an absolute upper limit on the number density $n(> M_\star, z)$ and stellar mass density $\rho_\star(> M_\star, z)$ of galaxies above a stellar mass limit of M_\star at any epoch z . The reported masses of the most massive galaxy candidates at $z \sim 10$ in *JWST* observations are in tension with these limits, indicating an issue with well-developed techniques for photometric selection of galaxies, galaxy stellar mass or effective survey volume estimates, or the Λ CDM model. That the strongest tension appears at $z \sim 10$, and not (yet?) at the highest redshifts probed by *JWST* galaxy candidates ($z \sim 16 - 20$), is promising for tests of the Λ CDM model using forthcoming wider-area *JWST* surveys.

Key words: cosmology: theory – galaxies: abundances – galaxies: high-redshift

1 INTRODUCTION

Λ CDM-like cosmological models share a similar basic assumption: baryons and dark matter are well-mixed at very early times, and as baryons collapse into dark matter halos, the maximum amount of baryonic material within a halo will be equal to $M_b = f_b M_{\text{halo}}$, where $f_b \equiv \Omega_b/\Omega_m$ is the cosmic baryon fraction. This, in turn bounds the total stellar content of a dark matter halo: $M_\star(M_{\text{halo}}) \leq M_b(M_{\text{halo}})$. In what follows, I show how this simple relation can be used as a stringent test of either cosmological models or of the reliability of photometric selection and physical characterization of high-redshift galaxy candidates. My analysis is in many ways similar to Behroozi & Silk (2018), who connected cumulative number densities of dark matter halos to high-redshift galaxy stellar mass functions, though I also consider the maximal cumulative stellar mass density allowed in Λ CDM. The question of the consistency of stellar mass functions and the underlying cosmological dark matter halo mass functions has become considerably more urgent since the very recent release of the first data from *JWST*, and with it, a swarm of high-redshift galaxy candidates (Atek et al. 2022; Castellano et al. 2022; Donnan et al. 2022; Finkelstein et al. 2022; Labbé et al. 2022; Morishita & Stiavelli 2022; Naidu et al. 2022; Yan et al. 2022).

2 ASSUMPTIONS

I adopt the base Λ CDM model of Planck Collaboration et al. (2020), which assumes no spatial curvature and initial conditions that are Gaussian and adiabatic, as the standard cosmological model. I use best fit values for cosmological parameters based on the Planck TT,TE,EE+lowE+lensing likelihood applied to the full-mission data. The relevant parameters and values for this work are the present-day

Hubble constant, $H_0 = 67.32 \text{ km s}^{-1} \text{ Mpc}^{-1}$; the $z = 0$ density parameter for matter, $\Omega_m = 0.3158$ (which includes baryons, dark matter, and non-relativistic neutrinos); the slope of the primordial power spectrum of density fluctuations, $n_s = 0.96605$; the rms amplitude of the linear matter power spectrum at $z = 0$ as measured in spheres of radius $8 h^{-1} \text{ Mpc}$, $\sigma_8 = 0.8120$; and the cosmic baryon fraction, $f_b \equiv \Omega_b/\Omega_m = 0.156$ (Planck Collaboration et al. 2020).

With these values, the linear matter power spectrum is specified at all times relevant for structure formation. The non-linear density field, home to the dark matter halos that host galaxies, must be computed numerically. However, a long line of research starting with Press & Schechter (1974) has been devoted to connecting the abundance of dark matter halos as a function of redshift and mass to the underlying linear matter power spectrum. In what follows, I use the Sheth & Tormen (1999) dark matter halo mass function $dn(M, z)/dM$ — the number of dark matter halos of mass M per unit mass per unit comoving volume at redshift z — to compute the comoving number density of halos above a given halo mass threshold,

$$n(> M_{\text{halo}}, z) = \int_{M_{\text{halo}}}^{\infty} dM \frac{dn(M, z)}{dM} \quad (1)$$

and the comoving mass density in halos more massive than M_{halo} ,

$$\rho(> M_{\text{halo}}, z) = \int_{M_{\text{halo}}}^{\infty} dM M \frac{dn(M, z)}{dM}. \quad (2)$$

These translate directly to upper limits on the number density of galaxies having stellar mass above a threshold value M_\star , $n(> M_\star, z)$, and stellar mass density of galaxies above M_\star as a function of M_\star and z , $\rho_\star(> M_\star, z)$. In both cases, the limits come from the straightforward assumption that $M_\star = \epsilon f_b M_{\text{halo}}$, with $\epsilon \leq 1$ being the efficiency of converting baryons into stars. For $\epsilon = 1$, we have $M_\star = M_{\star, \text{max}} = f_b M_{\text{halo}}$, the largest stellar content a halo can have given its cosmic allotment of baryons.

^{*} mbk@astro.as.utexas.edu

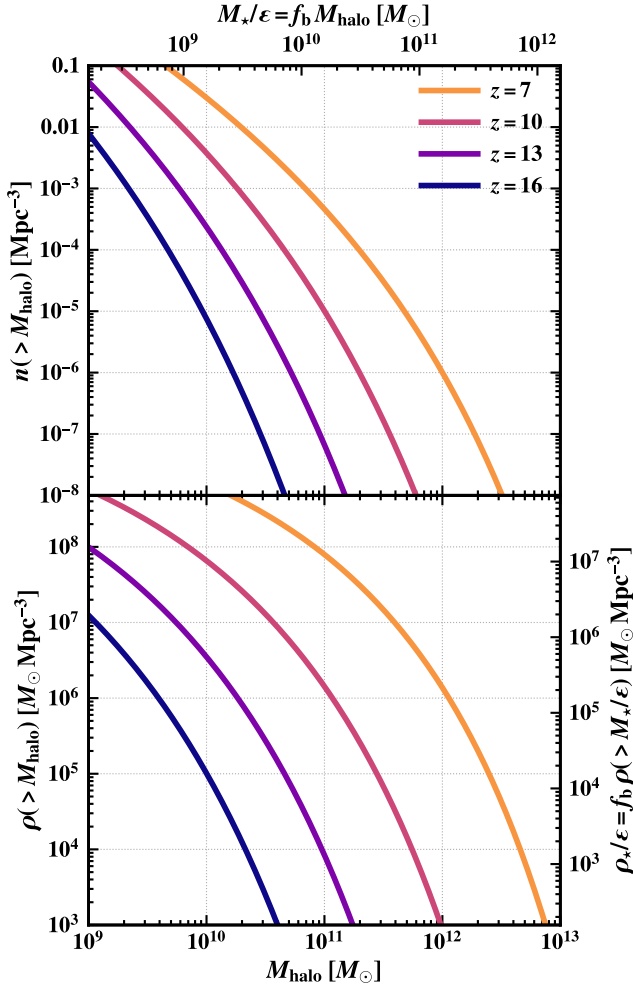


Figure 1. The cumulative comoving number density (top) and mass density (bottom) of halos more massive than M_{halo} at various redshifts. The secondary x -axis (top) shows the maximal stellar mass given M_{halo} , $M_{\star, \text{max}} = f_b M_{\text{halo}}$, while the secondary y -axis on the bottom plot shows the upper limit to the comoving stellar mass density contained in galaxies more massive than $M_{\star, \text{max}}$. Galaxies, or populations of galaxies, at a given redshift must lie below the curves for that redshift in both the upper and lower plots, modulo observational errors and sample variance considerations, in Λ CDM. Detection of a galaxy or population of galaxies at redshift z lying above the curve corresponding to that redshift in either panel indicates potential tension with Λ CDM predictions.

3 RESULTS

Figure 1 shows the cumulative comoving number density of dark matter halos (top) and the density of collapsed mass contained in halos more massive than M_{halo} as a function of M_{halo} (bottom) at $z = 7, 10, 13,$ and 16 . Both functions evolve strongly with redshift: for example, the cumulative number density and mass density contained in halos more massive than $10^{11} M_{\odot}$ increase by more than a factor of 10^4 from $z = 16$ to $z = 7$. The evolution at higher mass thresholds is increasingly strong. The upper x -axis shows the associated maximum stellar content $M_{\star, \text{max}}$ at each halo mass; if $\epsilon < 1$, a galaxy will move to the right on these plots (i.e., it must be hosted by a higher-mass halo, which is intrinsically rarer). The right-hand y -axis on the lower plot shows the maximum stellar mass density $\rho_{\star, \text{max}}/\epsilon = f_b \rho(>$

$M_{\text{halo}})$ contained in halos more massive than M_{halo} (or galaxies more massive than $M_{\star, \text{max}}/\epsilon$).

The cumulative comoving number density of dark matter halos more massive than M_{halo} sets an upper limit on the comoving number density of galaxies more massive than M_{\star} since at least $f_b M_{\text{halo}}$ worth of baryons is required to form a galaxy of mass M_{\star} . Roughly speaking, it is unlikely in a survey of volume V to find a galaxy whose stellar mass exceeds the value corresponding to $n(> M_{\star, \text{max}}) \approx V^{-1}$. Similarly, the cumulative comoving density of collapsed mass sets an upper limit on the density of collapsed baryons, $\rho_b(> M_{\text{halo}}) = f_b \rho(> M_{\text{halo}})$, which in turn sets a strict upper limit on the comoving mass density of stars contained in halos more massive than M_{halo} .

$$\rho_{\star}(> M_{\text{halo}}) \leq f_b \rho(> M_{\text{halo}}), \quad (3)$$

and the density of stars contained in galaxies above a given M_{\star} ,

$$\rho_{\star}(> M_{\star}) \leq f_b \rho(> M_{\star}/f_b). \quad (4)$$

The left panel of Figure 2 shows the relationship between inferred stellar mass $M_{\star, \text{max}}$ (i.e., assuming $\epsilon = 1$) and redshift for fixed cumulative comoving number densities ranging from 10^{-8} Mpc^{-3} (dark blue) to 10^{-2} Mpc^{-3} (yellow). The lighter (darker) gray line corresponds to rarer halos with $n(> M_{\text{halo}})/\text{Mpc}^{-3} = 10^{-10}$ (10^{-9}). The curves evolve rapidly with redshift, with the mass corresponding to a fixed cumulative comoving number density increasing by two orders of magnitude from $z = 20$ to $z = 8$. This rapid rise indicates that the mass reservoir available for the most massive galaxies increases quickly and that, to first order, the most massive galaxies at $z = 20$ should be significantly less massive than the most massive galaxies at $z = 10$ (however, hierarchical assembly guarantees that individual halo mass accretion histories are flatter than these curves). The stars on the plot show several of the high-redshift galaxy candidates detected in *JWST* observations (from Atek et al. 2022; Donnan et al. 2022; Finkelstein 2016; Labbé et al. 2022; Naidu et al. 2022) that are intrinsically rare in terms of their stellar content at that redshift; the candidates must be hosted by halos with cumulative comoving number densities that are *at most* $10^{-2} - 10^{-8} \text{ Mpc}^{-3}$ and could be significantly smaller.

The two most massive high-redshift galaxy candidates from the Labbé et al. (2022) sample, at $z \approx 10$ and $z \approx 7.5$, are each approximately $M_{\star} = 10^{11} M_{\odot}$ and are shown as blue stars. These objects are unexpectedly massive: the $z = 10$ ($z = 7.5$) candidate has a stellar content reflective of halos that have cumulative number densities no higher than $\approx 10^{-8}$ ($10^{-6.4}$) Mpc^{-3} even though they were found in a survey of 40 arcmin^2 (4 NIRCcam fields), which is a volume of $V \approx 10^5 \text{ Mpc}^3$ at $z = 10 \pm 1$. Put another way, the most massive object we would expect to see, on average, in a volume like this has a comoving number density of $\sim V^{-1} \approx 10^{-5} \text{ Mpc}^{-3}$; it would typically require a survey that is 10^3 times larger in area to find an object with number density of 10^{-8} Mpc^{-3} (the *maximum* possible number density for the $z = 9.9$ candidate; see also Labbé et al. 2022). Again, assuming a more realistic conversion efficiency of $\epsilon < 1$ would move these constraints to yet lower number densities (the halos would have to be a factor of $1/\epsilon$ more massive), which fall off quickly with decreasing ϵ (increasing host halo mass): for an efficiency of $\epsilon = 0.316$, the $z = 10$ ($z = 7.5$) candidate corresponds to a halo with a cumulative comoving number density of at most 3×10^{-11} (3×10^{-9}) Mpc^{-3} .

The right panel of Figure 2 shows the cumulative stellar mass density reported by Labbé et al. (2022) for two stellar mass thresholds at $z \approx 10$. The data, which come from a handful of massive objects, provide a strong discrepancy with Λ CDM expectations even in the most optimistic scenario: both points fall in the regime where the measured

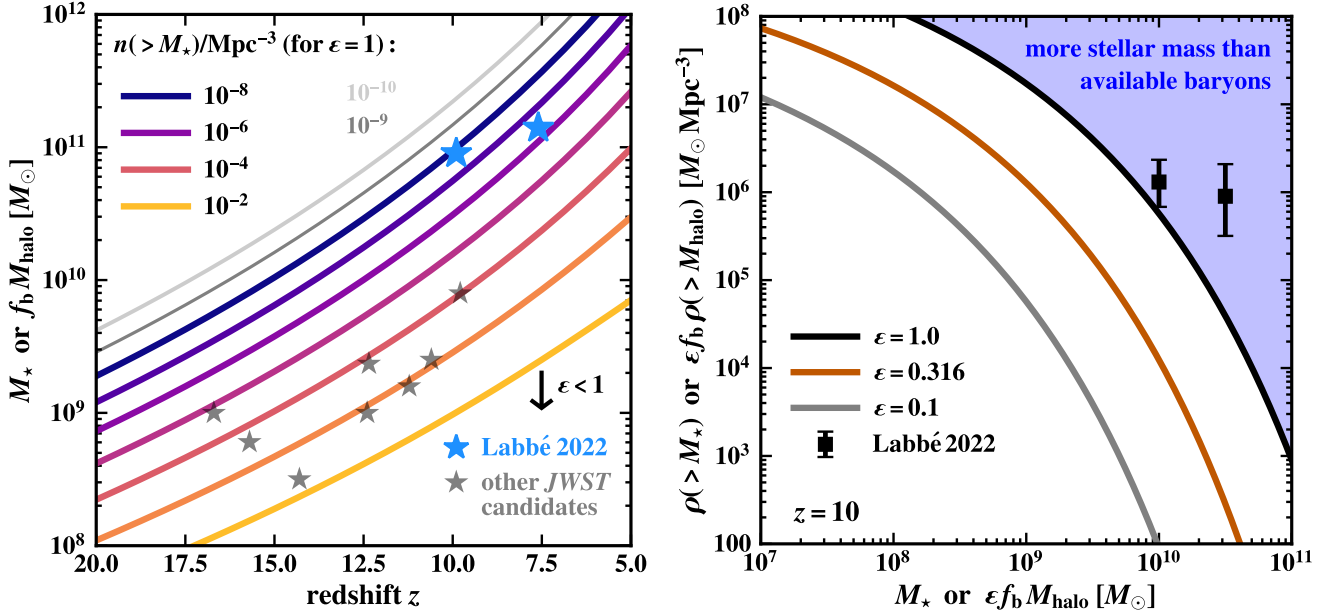


Figure 2. *Left:* The relationship between $M_{\star, \text{max}}$ and redshift for a variety of fixed cumulative comoving number densities, from 10^{-8}Mpc^{-3} (dark blue) to 10^{-3}Mpc^{-3} (orange). The existence of a galaxy with M_\star at a given redshift z requires that such galaxies have a cumulative comoving number density that is at most the number density shown on this plot, as those galaxies must reside in host halo of mass $M_{\text{halo}} = M_\star / (f_b \epsilon)$. The cumulative comoving number density corresponding to an observed M_\star will likely be (much) smaller than as indicated here, as the plot assumes the physically maximal $\epsilon = 1$. For smaller values of ϵ , the curves move down relative to the points by a factor of ϵ (as indicated by the black downward-facing arrow). Also shown are high-redshift galaxy candidates found in *JWST* data (blue and grey stars). *Right:* The comoving stellar mass density contained within galaxies more massive than M_\star at $z = 10$ for three values of the assumed conversion efficiency ϵ of a halo’s cosmic allotment of baryons into stars. Even assuming that *all* available baryons in all halos with enough baryons to form 10^{10} or $10^{10.5} M_\odot$ of stars at $z = 10$ have indeed been converted into stars by that point — an unrealistic limit — it is still not possible to produce the stellar mass density measured by Labbé et al. (2022) in Λ CDM with a Planck 2020 cosmology (ignoring sample variance considerations). For more realistic values of ϵ , the discrepancy is substantially larger. The right-most data point exceeds the maximal Λ CDM expectation by more than a factor of 20, meaning a large correction to the inferred stellar mass or effective volume of the sample is required to bring observation and theory into agreement.

stellar mass density exceeds the theoretical limit of $f_b \rho(> M_{\text{halo}})$, though the point at $M_\star = 10^{10} M_\odot$ is marginally consistent when considering the 1σ error. Assuming a more reasonable conversion efficiency for available baryons into stars of $\epsilon \equiv M_\star / (f_b M_{\text{halo}}) = 0.1$ or 0.316 results in a significantly stronger discrepancy. While the comparison in the left panel shows that the Labbé et al. (2022) candidates are much more common — by a factor of 1000 for the $z = 10$ object — than expected in Λ CDM, the discrepancy in the right panel is more grievous, as it originates from collections of galaxies that are less subject to the statistics of the rarest individual objects.

4 DISCUSSION

The first glimpse of high-redshift galaxy formation with *JWST* has revealed perhaps surprisingly massive galaxies at early times. These systems provide a way to test a bedrock property of the Λ CDM model (or, e.g., assumptions in derivations of stellar masses or the viability of high-redshift galaxy candidates): the stellar content of halos should not exceed the available baryonic material in those halos. This requirement does not rely on assumptions such as abundance matching but rather is simply a statement about the baryonic reservoir associated with halos that contain enough baryonic material to form the galaxies in question. It is also more stringent than the requirement that the observed galaxy UV luminosity function not exceed the theoretical maximum coming from a nearly instantaneous (10 Myr) conversion of a halo’s full baryonic reservoir into stars (Mason et al. 2022), as it is an integral constraint as opposed to a differential one.

The massive, high-redshift galaxy candidates cataloged in Labbé et al. (2022) appear to violate the integral constraints in terms of their cumulative number densities and stellar mass densities.

The discrepancy between the observed high-redshift galaxy candidates and Λ CDM expectations is robust to choice of halo mass function parameterization and cosmological parameters for the base Λ CDM model: if anything, the Sheth & Tormen (1999) mass function may over-estimate the abundance of massive halos at high redshifts (Wang et al. 2022). Intriguingly, models with enhanced values of σ_8 and the physical matter density $\Omega_m h^2$ — such as some Early Dark Energy models whose aim is to resolve the Hubble Tension (e.g., Smith et al. 2022) — come closer to producing the requisite baryonic reservoirs for obtaining the most massive Labbé et al. candidates, though the stellar mass density in the highest M_\star bin still exceeds the theoretical maximum by a factor of ~ 5 (or $\sim 80\%$ when considering the 1σ error) in this model. Sample variance is certainly an issue for the relatively small 40 arcmin^2 size of the fields from which the candidates were drawn, but the magnitude of the discrepancy is large enough that it is difficult to appeal to sample variance to explain the full effect. Whether this points to an issue with the presumed properties (such as stellar masses or effective volumes) of the galaxy candidates or with the underlying cosmology remains to be seen. If these massive galaxies are spectroscopically confirmed, and/or if other galaxies with similar properties at $z \gtrsim 10$ are found, they will present a serious challenge for Λ CDM structure formation with parameters given by Planck Collaboration et al. (2020) because they signify the existence of a significantly larger reservoir of collapsed baryons than is possible in Λ CDM. It is noteworthy that the

strongest tension in Figure 2 appears at $z \sim 10$ and not at the highest redshifts of reported galaxy candidates ($z \sim 16 - 20$): forthcoming wider-field *JWST* surveys should be able to quickly confirm or refute the existence of this tension. If future *JWST* data continue to reveal the presence of strikingly massive galaxies at very early cosmic epochs, more exciting surprises lie ahead for the fields of galaxy formation and cosmology.

DATA AVAILABILITY

All data going into the calculations and figures are freely available upon request to the author; sharing of the data from [Labbé et al. \(2022\)](#) is subject to permission from the authors of that work.

ACKNOWLEDGMENTS

This paper is dedicated to the memory of Steven Weinberg, who would have been thrilled to see how well *JWST* is working and excited to learn what it will reveal about cosmology and galaxy formation across a variety of cosmic epochs. I thank Pieter van Dokkum and Ivo Labbé for sharing data from [Labbé et al. \(2022\)](#) and Steve Finkelstein, Pawan Kumar, and Dan Weisz for helpful discussions. I apologize for not being able to keep this draft to a maximum of 2 pages, which was my original goal. I acknowledge support from the University of Texas at Austin through the Faculty Research Assignment program, NSF CAREER award AST-1752913, NSF grants AST-1910346 and AST-2108962, NASA grant 80NSSC22K0827, and HST-AR-15809, HST-GO-15658, HST-GO-15901, HST-GO-15902, HST-AR-16159, and HST-GO-16226 from the Space Telescope Science Institute, which is operated by AURA, Inc., under NASA contract NAS5-26555. I am very grateful to the developers of the python packages that I used in preparing this paper: NUMPY ([Harris et al. 2020](#)), SCIPY ([Virtanen et al. 2020](#)), MATPLOTLIB ([Hunter 2007](#)), HMF ([Murray et al. 2013](#); [Murray 2014](#)), and IPYTHON ([Pérez & Granger 2007](#)). This research has made extensive use of NASA's Astrophysics Data System (<http://adsabs.harvard.edu/>) and the arXiv e-Print service (<http://arxiv.org>).

REFERENCES

- Atek H., Shuntov M., Furtak L. J., Richard J., Kneib J.-P., Mahler A., Zitrin G., McCracken Clotilde Laigle Stéphane Charlot H. J., 2022, arXiv:2207.12338 [astro-ph], p. [arXiv:2207.12338](#)
- Behroozi P., Silk J., 2018, *MNRAS*, **477**, 5382
- Castellano M., et al., 2022, arXiv:2207.09436 [astro-ph], p. [arXiv:2207.09436](#)
- Donnan C. T., et al., 2022, arXiv:2207.12356 [astro-ph], p. [arXiv:2207.12356](#)
- Finkelstein S. L., 2016, *Publ. Astron. Soc. Australia*, **33**, e037
- Finkelstein S. L., et al., 2022, arXiv:2207.12474 [astro-ph], p. [arXiv:2207.12474](#)
- Harris C. R., et al., 2020, *Nature*, **585**, 357
- Hunter J. D., 2007, *Computing In Science & Engineering*, **9**, 90
- Labbé I., et al., 2022, arXiv:2207.12446 [astro-ph], p. [arXiv:2207.12446](#)
- Mason C. A., Trenti M., Treu T., 2022, arXiv:2207.14808 [astro-ph], p. [arXiv:2207.14808](#)
- Morishita T., Stiavelli M., 2022, arXiv:2207.11671 [astro-ph], p. [arXiv:2207.11671](#)
- Murray S., 2014, HMF: Halo Mass Function calculator, Astrophysics Source Code Library, record ascl:1412.006 (ascl:1412.006)
- Murray S. G., Power C., Robotham A. S. G., 2013, *Astronomy and Computing*, **3**, 23
- Naidu R. P., et al., 2022, arXiv:2207.09434 [astro-ph], p. [arXiv:2207.09434](#)
- Pérez F., Granger B. E., 2007, *Computing in Science and Engineering*, **9**, 21

- Planck Collaboration et al., 2020, *A&A*, **641**, A6
- Press W. H., Schechter P., 1974, *ApJ*, **187**, 425
- Sheth R. K., Tormen G., 1999, *MNRAS*, **308**, 119
- Smith T. L., Lucca M., Poulin V., Abellan G. F., Balkenhol L., Benabed K., Galli S., Murgia R., 2022, arXiv:2202.09379 [astro-ph], p. [arXiv:2202.09379](#)
- Virtanen P., et al., 2020, *Nature Methods*, **17**, 261
- Wang Q., Gao L., Meng C., 2022, arXiv:2206.06313 [astro-ph], p. [arXiv:2206.06313](#)
- Yan H., Ma Z., Ling C., Cheng C., Huang J.-s., Zitrin A., 2022, arXiv:2207.11558 [astro-ph], p. [arXiv:2207.11558](#)